Multiplexing schemes for optical communication through atmospheric turbulence

Liliana Borcea*   Josselin Garnier†   Knut Sølna‡

December 6, 2019

Abstract

A central question in free-space optical communications is how to improve the transfer of information between a transmitter and receiver. The capacity of the communication channel can be increased by multiplexing of independent modes using either: (1) the MIMO (Multiple-Input-Multiple-Output) approach, where the communication is done with modes obtained from the singular value decomposition of the transfer matrix from the transmitter array to the receiver array, or (2) the OAM (Orbital Angular Momentum) approach, which uses vortex beams that carry angular momenta. In both cases, the number of usable modes is limited by the finite aperture of the transmitter and receiver, and the effect of the turbulent atmosphere. The goal of this paper is twofold: First, we show that the MIMO and OAM multiplexing schemes are closely related. Specifically, in the case of circular apertures, the usable singular modes of the transfer matrix are essentially the same as the commonly used Laguerre-Gauss vortex beams, provided these have a special radius that depends on the wavelength, the distance from the transmitter to the receiver and the ratio of the radii of their apertures. Second, we study the effect of atmospheric turbulence on the communication modes using the phase screen method put in the mathematical framework of beam propagation in random media.

1 Introduction

In free-space optical communications, one seeks to transfer information between a transmitter array and a receiver array using laser beams. It is an important technology for line-of-sight communication between moving locations (e.g. in satellite communication), or for settings where fiber-based systems do not exist.

---

*Department of Mathematics, University of Michigan, Ann Arbor, MI 48109. `borcea@umich.edu`

†Centre de Mathématiques Appliquées, Ecole Polytechnique, 91128 Palaiseau Cedex, France. `josselin.garnier@polytechnique.edu`

‡Department of Mathematics, University of California at Irvine, Irvine, CA 92697. `ksolna@math.uci.edu`

A central question is how to increase the capacity of the communication channel via multiplexing independent sub-channels called modes. Typically, these are defined as special orthogonal solutions of the Helmholtz equation in homogeneous transmission media. Orbital Angular Momentum (OAM) beams [9, 2] are such solutions, also known as vortex beams [8, Chapter 2], because they exhibit a vortex on the axis of the beam, where the intensity is zero and the phase is not defined. Popular examples of OAM beams are: (1) Bessel beams, which have the desirable nondiffractive property, but cannot be realized in practice as they carry infinite energy [3]. Therefore, they are approximated via some truncation strategy to obtain, for example, the Bessel-Gauss beams [10]. (2) Hermite-Gauss and Laguerre-Gauss beams [20, Section 16], which are solutions of the paraxial approximation of the Helmholtz equation in rectangular and cylindrical coordinates, respectively. The Laguerre-Gauss beams are of special interest because they are easily realizable in practice [1, 23].

OAM beams have received much attention because by changing their azimuthal angle θ dependency $\exp(ij\theta)$, where the integer j is the so-called topological charge, one can create in theory an infinite number of modes. However, the number of usable modes is limited in practice by the finite size of the apertures of the transmitter and receiver, the interaction of the beam with the atmosphere and noise. If these factors are not taken into account, then the modes are no longer orthogonal at the receiver end, meaning that there is channel cross-talk and loss of information [1, 5].

The finite aperture size can be accounted for by using a Singular Value Decomposition (SVD) based Multiple-Input-Multiple-Output (MIMO) multiplexing approach, where the modes are singular vectors of the transfer matrix [13]. The transmission modes are the right singular vectors and the received modes are the left singular vectors. The SVD gives the optimal useable communication modes, corresponding to the significant singular values. Ideally, these modes should be determined by measuring the transfer matrix and then carrying out its SVD decomposition. However, the atmosphere changes in time and repeated measurements of the transfer matrix may be difficult to make in practice. This has motivated studies like [1, 5, 18], which seek to quantify with numerical simulations the effect of atmospheric turbulence on modes calculated for a proxy transfer matrix in a synthetic homogeneous medium.

A much debated issue has been the advantage of using OAM beams versus MIMO multiplexing [4, 6, 14]. Here we show that in fact the two approaches are closely related. We consider a paraxial beam propagation model and assume that we can approximate the transmission and receiver arrays by continuous disk shaped apertures. Then, the SVD of the proxy transfer matrix has an explicit solution in terms of the circular prolate spheroidal functions [21, 12]. If we let a_R and a_T be the radii of the receiver and transmitter arrays, and denote by λ the wavelength and L the transmission distance, the matrix has

$$N = \frac{\pi a_R^2}{[\lambda L/(2a_T)]^2} \tag{1}$$

singular values that are very close to one, and the remaining ones plunge rapidly

toward zero. A large singular value means that the mode carries large power within the receiver aperture and is thus less affected by noise. Physically, the number N can be interpreted as the number of focal spots of linear size $\lambda L/(2a_T)$ that fit in the receiver aperture area πa_R^2. The interesting regime for communications corresponds to a large N, so that one can multiplex the many N useable modes.

It has been observed in [19, 17] that in the case of soft apertures, with Gaussian apodization, the convenient Laguerre-Gauss beams are the modes given by the SVD. The similarity of some Laguerre-Gauss beam modes and the circular prolate spheroidal functions was also noticed in [17, 13]. Using the theory of circular prolate spheroidal functions [21], we show that in fact the Laguerre-Gauss beam modes are the significant modes given by the SVD even for hard aperture thresholding, as long as their radius is carefully calibrated in terms of the wavelength λ, the propagation distance L, and the ratio a_T/a_R as prescribed by the forthcoming formula (15).

Some recent studies [5] have found that Bessel-Gauss OAM beams are more robust to turbulence effects than the Laguerre-Gauss beams. Here we show that, provided the Laguerre-Gauss beams are calibrated as stated above, the opposite is true. We study the effect of turbulence using the mathematical theory of paraxial wave propagation in random media with statistics corresponding to Kolmogorov type turbulence. We use the theory to put numerical phase screen simulation results [16, 22] in a mathematical framework and to clarify the link between the phase screen parameters and the turbulence model.

The paper is organized as follows. In Section 2 we consider laser beam propagation in homogeneous free space and study different candidates to multiplexing schemes. In particular, we identify the leading singular vectors of the transfer matrix that are used in the MIMO approach and show that they are related to Gauss-Laguerre modes. In Section 3 we consider laser beam propagation through the turbulent atmosphere and give the Itô-Schrödinger mathematical model which characterizes the statistics of the transmitted beams. In Section 4 we quantify the robustness of different multiplexing schemes with respect to the turbulent atmosphere. We conclude with a brief summary in section 5.

2 Homogeneous paraxial wave equation

In this section we describe classical beams that exhibit orthogonality when they propagate through a homogeneous medium. They are approximate solutions of the Helmholtz equation of the form $u(r, \theta, z) \exp(ikz)$, with $u(r, \theta, z)$ satisfying the paraxial wave equation [20],

$$2ik\partial_z u(r, \theta, z) + \Delta_\perp u(r, \theta, z) = 0, \tag{2}$$

where $k = 2\pi/\lambda$ is the wavenumber. Because we assume circular apertures of the transmitter and receiver arrays, we use the cylindrical coordinates (r, θ, z), with z measured along the axis of the beam, radius r and azimuth θ. The operator $\Delta_\perp = r^{-1}\partial_r(r\partial_r \cdot) + r^{-2}\partial_\theta^2$ is the transverse Laplacian. We assume

throughout an input beam profile $u(r, \theta, z = 0)$ with slow variation with respect to λ, so that the paraxial approximation is valid.

2.1 Bessel-Gauss beams

Let $\beta > 0$ and $r_o > 0$ be such that $k \gg \beta$ and $kr_o \gg 1$. For any integer j, the input profile of the j-th Bessel-Gauss beam is [8, Section 12.1]

$$u_j^{\mathrm{BG}}(r, \theta, z = 0) = J_j(\beta r) \exp\left(-\frac{r^2}{r_o^2}\right) \exp\left(ij\theta\right), \tag{3}$$

where J_j is the Bessel function of the first kind. After propagation over a distance z in the homogeneous medium, the output profile is

$$u_j^{\mathrm{BG}}(r, \theta, z) = \frac{r_o}{r_z} J_j\left(\frac{\beta r}{1 + i\frac{z}{z_{\mathrm{R}}}}\right) \exp\left[\left(r^2 + \frac{\beta^2 z^2}{k^2}\right)\left(-\frac{1}{r_z^2} + i\frac{k}{2R_z}\right)\right]$$

$$\times \exp\left[ij\theta - i\frac{\beta^2}{2k}z - i\operatorname{atan}\left(\frac{z}{z_{\mathrm{R}}}\right)\right], \tag{4}$$

where $z_{\mathrm{R}} = kr_o^2/2$ is the Rayleigh length, r_z, resp. R_z, is the radius of a standard Gaussian beam at distance z, resp. the radius of curvature of the wavefront:

$$r_z = r_o\left(1 + \frac{z^2}{z_{\mathrm{R}}^2}\right)^{\frac{1}{2}}, \quad R_z = z\left(1 + \frac{z_{\mathrm{R}}^2}{z^2}\right). \tag{5}$$

If $r_o \to +\infty$ then (4) tends to

$$u_j(r, \theta, z) = J_j(\beta r) \exp\left(ij\theta - i\frac{\beta^2}{2k}z\right),$$

the ideal j-th Bessel beam [8, Section 12.1] which is diffraction-free, but cannot be realized in practice as it has infinite energy (L^2-norm).

2.2 Laguerre-Gauss beams

Let $r_o > 0$ be such that $kr_o \gg 1$ and p, j be integers with $p \geq 0$. The input profile of the (p, j)-th Laguerre-Gauss mode is [8, Section 2.2]

$$u_{p,j}^{\mathrm{LG}}(r, \theta, z = 0) = \sqrt{\frac{2p!}{\pi(|j| + p)!}}\left(\frac{\sqrt{2}r}{r_o}\right)^{|j|} L_p^{|j|}\left(\frac{2r^2}{r_o^2}\right)$$

$$\times \exp\left(-\frac{r^2}{r_o^2} + ij\theta\right), \tag{6}$$

where L_p^j is the generalized Laguerre polynomial $L_p^j(s) = \frac{e^s s^{-j}}{p!}\frac{d^p}{ds^p}\left(e^{-s}s^{p+j}\right)$. The input Laguerre-Gauss profiles are not compactly supported. However, their essential supports are disks with radii of the order of r_o for the low-order modes, and of the order $\sqrt{|j|}r_o$ for high mode indexes $|j|$ [15].

After propagation over a distance z in the homogeneous medium, the Laguerre-Gauss beam profiles are

$$
u_{p,j}^{\mathrm{LG}}(r,\theta,z) = \sqrt{\frac{2p!}{\pi(|j|+p)!}} \frac{r_o}{r_z} \left(\frac{\sqrt{2}r}{r_z}\right)^{|j|} L_p^{|j|}\left(\frac{2r^2}{r_z^2}\right)
$$

$$
\times \exp\left[r^2\left(-\frac{1}{r_z^2} + \frac{ik}{2R_z}\right)\right]
$$

$$
\times \exp\left[ij\theta - i(|j|+2p+1)\mathrm{atan}\left(\frac{z}{z_{\mathrm{R}}}\right)\right]. \tag{7}
$$

The beams widen due to diffraction, as modeled by the beam radius r_z and the radius R_z of curvature of the wavefront defined in (5).

2.3 SVD based MIMO multiplexing

Bessel-Gauss and Laguerre-Gauss beams are two of the many examples of orthogonal modes that carry an angular momentum i.e., a phase of the form $\exp(ij\theta)$ which is kept invariant during the propagation. In theory, for transmission through the homogeneous medium, and for infinite transmitter and receiver apertures, the countably infinite family of such orthogonal modes could be used to obtain an indefinite increase in the capacity of the communication channel. In reality, this cannot be achieved due to the finite transmitter and receiver apertures and heterogeneity in the transmission medium. We describe here the limitations imposed by the finite apertures and postpone until section 3 the discussion of the effect of a turbulent transmission medium.

A systematic approach for describing which beams are most appropriate for communication between a transmitter and receiver array is given by the SVD of the transfer matrix $\mathcal{T}$. Assuming that the transmitter array has n_T elements and the receiver array has n_R elements, this is an $n_R \times n_T$ matrix with complex entries $\mathcal{T}_{t,r}$ corresponding to the complex wave amplitude at the $r-$th receiver, due to a unit input at the $t-$th transmitter. The matrix $\mathcal{T}$ can be computed by solving the wave equation in the homogeneous medium. Its right singular vectors are the orthonormal input profiles that can be used in multiplexing at the transmitter array. The left singular vectors form the orthonormal basis that can be used for demultiplexing at the receiver array.

2.4 SVD in the continuum approximation

If the transmitters and receivers are closely spaced in the arrays with radii a_T and a_R, in the sense that their linear size is smaller than the Rayleigh resolution limit $\lambda L/[2\max\{a_T, a_R\}]$, we can approximate the arrays by the continuous apertures

$$
\mathcal{A}_{T,R} = \{\boldsymbol{x} = (r\cos\theta, r\sin\theta),\ 0 \le r \le a_{T,R},\ \theta \in [0, 2\pi]\}.
$$

In this continuous setting, the transfer matrix becomes the linear integral operator $\mathcal{T} : L^2(\mathcal{A}_T) \mapsto L^2(\mathcal{A}_R)$,

$$u(\boldsymbol{x}, L) = \mathcal{T} u_o(\boldsymbol{x}) = \int_{\mathcal{A}_T} u_o(\boldsymbol{x}') G\left((\boldsymbol{x}, L), (\boldsymbol{x}', 0)\right) d\boldsymbol{x}', \tag{8}$$

for $\boldsymbol{x} \in \mathcal{A}_R$, where $u_o(\boldsymbol{x}) = u(\boldsymbol{x}, 0)$ is the input beam profile at the transmitter array and the kernel is the Green's function of the paraxial equation (2),

$$G\left((\boldsymbol{x}, L), (\boldsymbol{x}', 0)\right) = \frac{k}{2i\pi L} \exp\left(i \frac{k|\boldsymbol{x} - \boldsymbol{x}'|^2}{2L}\right). \tag{9}$$

The right singular functions of $\mathcal{T}$, which define the transmission modes in the MIMO multiplexing, are of the form

$$u_o(\boldsymbol{x}) = \exp\left(-i \frac{k|\boldsymbol{x}|^2}{2L}\right) v\left(\frac{\boldsymbol{x}}{a_T}\right), \quad \boldsymbol{x} \in \mathcal{A}_T, \tag{10}$$

where $v(\boldsymbol{s})$ are the right singular functions of the linear integral operator $\mathcal{S} : L^2(B(\mathbf{0}, 1)) \mapsto L^2(B(\mathbf{0}, 1))$ defined by

$$\mathcal{S} v(\boldsymbol{s}) = \int_{B(\mathbf{0},1)} v(\boldsymbol{s}') \exp\left(-iC\boldsymbol{s} \cdot \boldsymbol{s}'\right) d\boldsymbol{s}', \qquad \boldsymbol{s} \in B(\mathbf{0}, 1), \tag{11}$$

with $B(\mathbf{0}, 1)$ the unit disk centered at the origin $\mathbf{0}$ of the cross-range plane and

$$C = \frac{k a_T a_R}{L}. \tag{12}$$

The operator $\mathcal{S}$ was studied by Slepian [21]. Its singular functions $v(\boldsymbol{s})$ are the generalized prolate spheroidal functions, its first $N = C^2/\pi$ singular values (recall (1)) are close to $1/C$, and the remaining ones plunge rapidly to zero.

We are interested in the case $C \gg 1$, where there are $N \gg 1$ transmission modes of the form (10) available for multiplexing. For such C, it follows from [21, Eq. (67)] that the leading singular functions of $\mathcal{S}$ behave like scaled Gauss-Laguerre functions

$$v_{p,j}(\boldsymbol{s}) = \exp\left(-\frac{C|\boldsymbol{s}|^2}{2}\right) L_p^{|j|}(C|\boldsymbol{s}|^2)(\sqrt{C}|\boldsymbol{s}|)^{|j|} e^{ij\arg(\boldsymbol{s})}, \tag{13}$$

for integers p, j, with $p \geq 0$. Thus, we conclude from (10) that the transmission modes are of the form (6) up to multiplicative constants,

$$u_{p,j}(\boldsymbol{x}, z = 0) = \exp\left(-i \frac{k|\boldsymbol{x}|^2}{2L} - \frac{|\boldsymbol{x}|^2}{r_o^2}\right) L_p^j\left(\frac{2|\boldsymbol{x}|^2}{r_o^2}\right) |\boldsymbol{x}|^j e^{ij\arg(\boldsymbol{x})}, \tag{14}$$

for the special radius
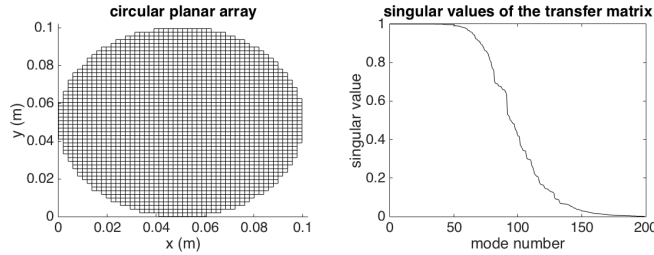
$$r_o = \frac{\sqrt{2L a_T}}{\sqrt{k a_R}}. \tag{15}$$

Figure 1: Left: Circular planar array with $n = 2063$ square elements with size 2mm in the disk shaped aperture $\mathcal{A}$ of radius $a = 5$cm. Right: The first 200 singular values of the transfer matrix for transmission distance $L = 1$km and wavelength $\lambda = 850$nm.

They correspond to the following leading singular values of $\mathcal{T}$ [21, Eq. (93)],

$$\mathfrak{S}_{p,j} = 1 - \mathfrak{S}'_{p,j}\big[1 + O(C^{-1})\big], \tag{16}$$

with

$$\mathfrak{S}'_{p,j} = \frac{\pi 2^{2|j|+4p+3} C^{|j|+2p+1} e^{-2C}}{p!(p+|j|)!}. \tag{17}$$

Note that the quadratic phase in the first factor in (14) makes the beam focus at distance (beam waist) $L/(1 + a_R^2/a_T^2)$. The beam then diffracts from there to the receiver array, to get an output profile that is similar to the emitted one, but rescaled by the radius a_R.

2.5   Illustration

We consider throughout a practical setup for free-space optical communication with laser beams [5] at wavelength $\lambda = 850$nm, using transmitter and receiver arrays with the same circular aperture $\mathcal{A}$, of radius $a = a_T = a_R = 5$cm. The arrays have $n = n_T = n_R = 2063$ square elements with side length 2mm (see left plot in Figure 1). The transmission distance is $L = 1$km. Note that the aperture is not centered at the origin $(0,0)$, but at $(5,5)$cm. All the beam axes are shifted to pass through this center.

The singular value decomposition described in section 2.4 is relevant here, because the Rayleigh resolution limit $\lambda_o L/(2a) = 8.5$mm is larger than the 2mm size of the elements of the arrays. After computing the $n \times n$ transfer matrix in the homogeneous medium and carrying out its SVD, we find the singular values displayed in the right plot in Figure 1. There are approximately 100 large ones, which is very close to the theoretical estimate (1) of the essential rank of the integral operator (8) that predicts $N = 109$. The right singular vectors give the orthonormal input profiles to be used in the MIMO multiplexing. The left singular vectors give the basis on which we project the wave at the receiver array, for demultiplexing. In our illustration the transmitter and receiver arrays are identical, so the transfer matrix is complex symmetric and the right

and left singular vectors are the same. We ensure that this is the case in the computations by using the symmetric (Takagi) SVD.
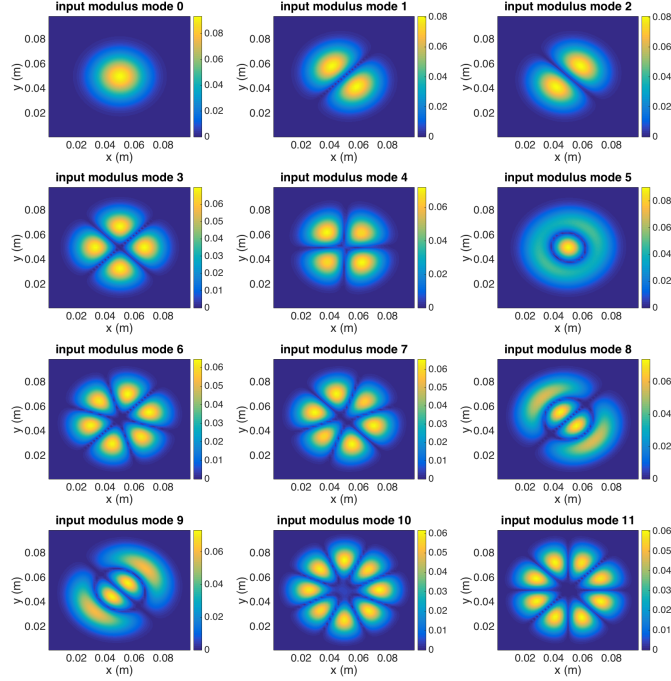

Figure 2: Moduli of the mode profiles. The axes are in meters.

The mode profiles are stepwise constant functions on the elements of the array, with values given by the singular vectors. We plot in Figure 2 the moduli of the first 12 modes. For comparison, we also display in Figure 3 the absolute values of the real and imaginary parts of the Laguerre-Gauss modes with initial radius $r_o = 1.64$cm calculated from (15). These modes are sorted according to their power fraction in $\mathcal{A}$. As expected from (14), the plots in Figures 2 and 3 are basically the same, aside from a rotation by the angle $\pi/4$, which is irrelevant because $\mathcal{A}$ is rotation invariant.

Eqs. (16-17) estimate the leading singular values, with corrections $\mathfrak{S}'_{p,j}$ displayed in Table 1. The sorting displayed in this table is the same as the sorting based on the power fraction in $\mathcal{A}$, used in Figure 3.

(p,j)	$(0,0)$	$(0,1)$	$(0,2)$	$(1,0)$	$(0,3)$	$(1,1)$	$(0,4)$
$\mathfrak{S}'_{p,j}$	$4\cdot 10^{-14}$	$3\cdot 10^{-12}$	10^{-10}	$2\cdot 10^{-10}$	$3\cdot 10^{-9}$	$8\cdot 10^{-9}$	$5\cdot 10^{-8}$

Table 1: Values of $\mathfrak{S}'_{p,j}$ sorted in increasing order.
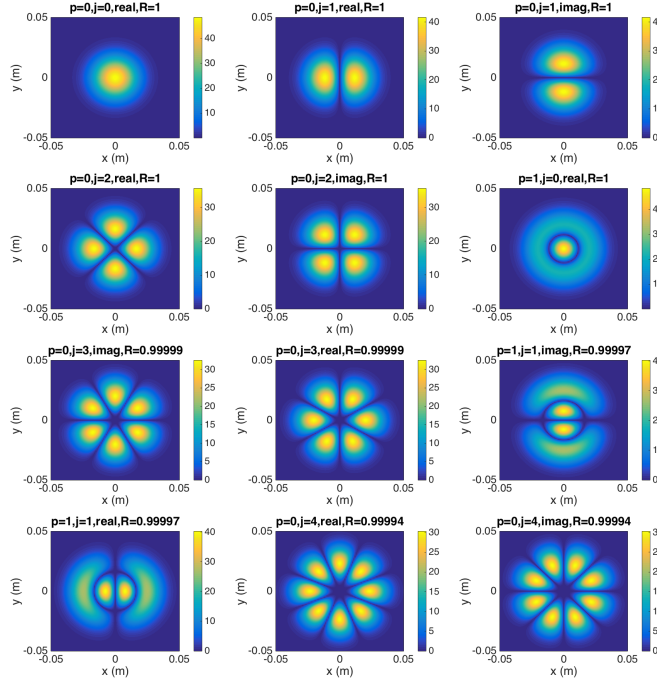
Figure 3: Absolute values of the real and imaginary parts of the Laguerre-Gauss modes with radius $r_o = 1.64$cm. The profiles are sorted according to the power fraction R in the transmitter aperture. The axes are in meters.

2.6 Discussion

The results in section 2.3 reconcile the MIMO approach, where the singular vectors of the transfer matrix are used for multiplexing, and the OAM approach, in which Laguerre-Gauss beams are used as transmission modes [8, section 6.2]. The useful modes correspond to the N large singular values or, equivalently, the Laguerre-Gauss beams with large power within the aperture, and they coincide for the two multiplexing approaches, provided that the initial radius r_o is chosen as in (15). Note that for this radius, the Rayleigh length satisfies $z_R = kr_o^2/2 = La_T/a_R$, so the larger the transmitter aperture, the smaller the diffraction effect.

At large mode numbers, corresponding to negligible power within the aperture, the Laguerre-Gauss modes and the singular vectors differ, because the latter are compactly supported in the aperture and the former extend outside the aperture. Obviously, such modes are not useful for transmitting information.

3 Communication through turbulence

The results in section 2 show that in the ideal case of transmission through a homogeneous medium, the leading N modes determined from the SVD decom-

position of the transfer matrix should be used as transmission modes. Moreover, these modes are the Laguerre-Gauss beams with initial radius (15) in the case of dense planar circular arrays and $N \gg 1$. We now seek to quantify how such a multiplexing scheme degrades in a turbulent transmission medium.

It was shown in [5] via numerical simulations, which do not account for finite transmitter and receiver apertures, that Bessel-Gauss beams outperform Laguerre-Gauss beams in channel efficiency through a turbulent medium. The earlier paper [16] studied the probability of detection of the angular momentum when a Laguerre-Gauss mode is transmitted through a turbulent medium by using a formal propagation model. A similar approach was used in [22], where the role of the turbulence strength measured in terms of the Fried parameter (relative to the aperture) was discussed. Further insight using this framework was provided in [18], where diffractive effects for relatively small aperture were discussed both from analytic and experimental viewpoints.

Here we present a framework where the role of the turbulence is taken into account in a rigorous fashion, and connect it to the phase screen model for numerical wave propagation. We also derive explicit formulas for the cross-correlations of the wave field in a specific scaling regime, corresponding to weak diffraction. These formulas give good predictions of the performance of MIMO and OAM multiplexing schemes, even for moderate diffraction, as explained in section 4.

3.1 Random paraxial wave equation and phase screen

Beam propagation through a turbulent medium can be described mathematically by the random paraxial wave equation

$$2ik\partial_z u(\boldsymbol{x}, z) + \Delta_\perp u(\boldsymbol{x}, z) + k^2 V(\boldsymbol{x}, z) u(\boldsymbol{x}, z) = 0, \tag{18}$$

for $\boldsymbol{x} \in \mathbb{R}^2$ and $z > 0$, with initial condition

$$u(\boldsymbol{x}, 0) = u_o(\boldsymbol{x}), \tag{19}$$

where $V(\boldsymbol{x}, z)$ is a random potential. We are interested in a phase screen method (i.e., a split-step Fourier method with grid step ℓ_z) for solving this equation. This amounts to assuming that the random potential is stepwise constant in z over intervals with length ℓ_z,

$$V(\boldsymbol{x}, z) = \sum_{n \geq 0} \mathbf{1}_{[n\ell_z, (n+1)\ell_z)}(z) V_n(\boldsymbol{x}). \tag{20}$$

Here $V_n(\boldsymbol{x})$ are i.i.d. copies of a stationary two-dimensional Gaussian, zero-mean random field with covariance function

$$\mathbb{E}[V_n(\boldsymbol{x}) V_n(\boldsymbol{x}')] = \mathcal{R}(\boldsymbol{x} - \boldsymbol{x}'). \tag{21}$$

We assume isotropic statistics, with covariance given by the Matérn model $\mathcal{R}(\boldsymbol{x}) = \mathcal{R}_\nu(|\boldsymbol{x}|)$,

$$\mathcal{R}_\nu(r) = \frac{\sigma^2}{\Gamma(\nu) 2^{\nu-1}} \left(\frac{2\sqrt{\nu} r}{\ell_c} \right)^\nu K_\nu \left(\frac{2\sqrt{\nu} r}{\ell_c} \right), \tag{22}$$

10

and power spectral density

$$\widehat{\mathcal{R}}(\boldsymbol{\kappa}) = \int_{\mathbb{R}^2} \mathcal{R}(\boldsymbol{x}) e^{-i\boldsymbol{\kappa}\cdot\boldsymbol{x}} d\boldsymbol{x} = \sigma^2 \frac{2^{2\nu+2}\pi\nu^{\nu+1}}{\ell_c^{2\nu}} \left(\frac{4\nu}{\ell_c^2} + |\boldsymbol{\kappa}|^2\right)^{-\nu-1}. \tag{23}$$

This model depends on three hyperparameters σ^2, ℓ_c, ν, and K_ν is the modified Bessel function of second kind. The hyperparameter $\nu \in [1/2, \infty)$ characterizes the smoothness of the process (the realizations are ν'-Hölder continuous, for any $\nu' < \nu$), $\sigma^2 = \mathcal{R}(\mathbf{0})$ is the variance and ℓ_c is the correlation radius. In the limit $\nu \to \infty$, we obtain from (22) the smooth Gaussian covariance model $\mathcal{R}(\boldsymbol{x}) = \sigma^2 \exp\left(-|\boldsymbol{x}|^2/\ell_c^2\right)$, whereas the other extreme $\nu = 1/2$ gives the rough exponential covariance model $\mathcal{R}(\boldsymbol{x}) = \sigma^2 \exp\left(-\sqrt{2}|\boldsymbol{x}|/\ell_c\right)$.

We consider henceforth $\nu = 5/6$, so that (22) gives a Kolmogorov-type model with outer scale proportional to ℓ_c and inner scale equal to zero. More explicitly, we recover from (23) the standard Kolmogorov model

$$\widehat{\mathcal{R}}(\boldsymbol{\kappa}) = 0.033 C_n^2 \left(\frac{1}{L_0^2} + |\boldsymbol{\kappa}|^2\right)^{-11/6},$$

if we set $\nu = 5/6$, $\ell_c = 2\sqrt{\nu}L_0$, and $\sigma^2 = 0.033 C_n^2 L_0^{2\nu}/(4\pi\nu)$. With this parameterization, L_0 is the outer scale of turbulence and C_n^2 is the turbulence strength. In Figure 4 we plot two realizations of a phase screen obtained with this model.
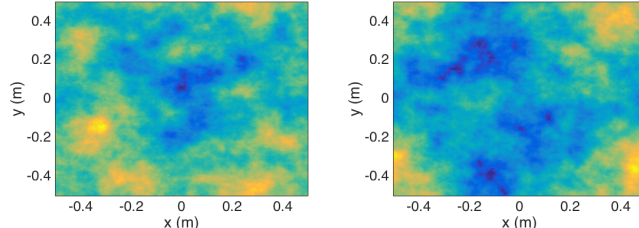

Figure 4: Two independent phase screens, with $\ell_c = 20$ cm ($L_0 = 37$ cm). The coordinates x and y in the cross-range plane are in meters.

3.2 Itô-Schrödinger model

It is proved in [7] that in the high frequency and long range regime $\lambda_o \ll \ell_c, r_o \ll L$, the statistical distribution of the solution of (18–19) can be approximated by that of the solution of the Itô-Schrödinger equation

$$du(\boldsymbol{x}, z) = \frac{i}{2k}\Delta_\perp u(\boldsymbol{x}, z)\, dz + \frac{ik}{2} u(\boldsymbol{x}, z) \circ dB(\boldsymbol{x}, z),$$

with initial condition (19). We wrote this equation in Stratonovich form, and $B(\boldsymbol{x}, z)$ is a Brownian field with covariance function

$$\mathbb{E}\left[B(\boldsymbol{x}, z)B(\boldsymbol{x}', z')\right] = \ell_z \mathcal{R}(\boldsymbol{x} - \boldsymbol{x}') \min\{z, z'\}.$$

11

The statistical moments of the beam can be calculated using Itô's formula [11]. The first moment models the coherent (mean) wave and satisfies the damped Schrödinger equation

$$\partial_z \mathbb{E}[u(\boldsymbol{x}, z)] = \frac{i}{2k} \Delta_\perp \mathbb{E}[u(\boldsymbol{x}, z)] - \frac{k^2 \sigma^2 \ell_z}{8} \mathbb{E}[u(\boldsymbol{x}, z)],$$

which can be solved explicitly to obtain

$$\mathbb{E}[u(\boldsymbol{x}, z)] = \int_{\mathbb{R}^2} u_o(\boldsymbol{x}') G\left((\boldsymbol{x}, z), (\boldsymbol{x}', 0)\right) d\boldsymbol{x}' \exp\left(-\frac{k^2 \sigma^2 \ell_z z}{8}\right). \quad (24)$$

The first factor (the integral) is the beam in the homogeneous medium propagated using the paraxial Green's function (9). The exponential decay models the loss of coherence of the beam due to scattering in the random medium.

The second moments of the beam can be described using the mean Wigner transform

$$\mathcal{W}(\boldsymbol{x}, \boldsymbol{\kappa}, z) = \int_{\mathbb{R}^2} \exp\left(-i\boldsymbol{\kappa} \cdot \boldsymbol{y}\right) \mathbb{E}\left[u\left(\boldsymbol{x} + \frac{\boldsymbol{y}}{2}, z\right) \overline{u}\left(\boldsymbol{x} - \frac{\boldsymbol{y}}{2}, z\right)\right] d\boldsymbol{y}, \quad (25)$$

where the bar denotes complex conjugate. This satisfies the radiative transport equation [7]

$$\partial_z \mathcal{W}(\boldsymbol{x}, \boldsymbol{\kappa}, z) + \frac{\boldsymbol{\kappa}}{k} \cdot \nabla_{\boldsymbol{x}} \mathcal{W}(\boldsymbol{x}, \boldsymbol{\kappa}, z) = \frac{k^2 \ell_z}{4(2\pi)^2} \int_{\mathbb{R}^2} \widehat{\mathcal{R}}(\boldsymbol{\kappa} - \boldsymbol{\kappa}')$$

$$\times \left[\mathcal{W}(\boldsymbol{x}, \boldsymbol{\kappa}', z) - \mathcal{W}(\boldsymbol{x}, \boldsymbol{\kappa}, z)\right] d\boldsymbol{\kappa}', \quad (26)$$

which can be solved explicitly

$$\mathcal{W}(\boldsymbol{x}, \boldsymbol{\kappa}, z) = \frac{1}{(2\pi)^2} \iint_{\mathbb{R}^2 \times \mathbb{R}^2} \widehat{\mathcal{W}}_o(\boldsymbol{\zeta}, \boldsymbol{y}) \exp\left[i\boldsymbol{\zeta} \cdot \left(\boldsymbol{x} - \boldsymbol{\kappa}\frac{z}{k}\right)\right]$$

$$\times \exp\left[-i\boldsymbol{\kappa} \cdot \boldsymbol{y} + \frac{k^2 \ell_z}{4} \int_0^z \mathcal{R}\left(\boldsymbol{y} + \boldsymbol{\zeta}\frac{z'}{k}\right) - \mathcal{R}(\boldsymbol{0}) dz'\right] d\boldsymbol{\zeta} d\boldsymbol{y}, \quad (27)$$

for $\widehat{\mathcal{W}}_o$ defined in terms of the initial beam profile (19) by

$$\widehat{\mathcal{W}}_o(\boldsymbol{\zeta}, \boldsymbol{y}) = \int_{\mathbb{R}^2} \exp(-i\boldsymbol{\zeta} \cdot \boldsymbol{x}) u_o\left(\boldsymbol{x} + \frac{\boldsymbol{y}}{2}\right) \overline{u_o}\left(\boldsymbol{x} - \frac{\boldsymbol{y}}{2}\right) d\boldsymbol{x}. \quad (28)$$

3.3 Weakly diffraction regime

If the initial radius r_o of the beam and the correlation radius ℓ_c satisfy the scaling relations $kr_o^2 \gg z$ and $k\ell_c^2 \gg z$, we have a weak diffraction regime, where the expressions of the first and second moments of the beam simplify to

$$\mathbb{E}[u(\boldsymbol{x}, z)] = u_o(\boldsymbol{x}) \exp\left(-\frac{k^2 \sigma^2 \ell_z z}{8}\right), \quad (29)$$

and

$$\mathbb{E}\Big[u\Big(\boldsymbol{x}+\frac{\boldsymbol{y}}{2},z\Big)\overline{u}\Big(\boldsymbol{x}-\frac{\boldsymbol{y}}{2},z\Big)\Big] = u_o\Big(\boldsymbol{x}+\frac{\boldsymbol{y}}{2}\Big)\overline{u_o}\Big(\boldsymbol{x}-\frac{\boldsymbol{y}}{2}\Big)$$
$$\times \exp\Big[\frac{k^2\ell_z z}{4}\big(\mathcal{R}(\boldsymbol{y})-\mathcal{R}(\boldsymbol{0})\big)\Big]. \tag{30}$$

This corresponds to multiplying the initial beam profile $u_o(\boldsymbol{x})$ with a global phase screen.

4 Demultiplexing and channel efficiency

We now use the results in section 3 to quantify the recovery of a single mode transmitted through a turbulent random medium. The recovery (demultiplexing) amounts to projecting the received wave field onto the basis of the transmitted modes and looking at the detected powers. We compare the efficiencies of the different orthogonal beam families discussed in Section 2. We use throughout the setup described in section 2.5, where the apertures of the transmitter and receiver arrays are the same disk $\mathcal{A}$ of radius a.

4.1 SVD based multiplexing

For the SVD based MIMO scheme, suppose that the transmitter array transmits the j-th homogeneous input mode $u(\boldsymbol{x}, z = 0) = u_j^{\mathrm{IN}}(\boldsymbol{x})$ for $j \geq 0$, and the receiver array projects the beam $u(\boldsymbol{x}, z = L)$ transmitted through the turbulent medium onto the homogeneous output modes $u_l^{\mathrm{OUT}}(\boldsymbol{x})$, for $l \geq 0$. The projection coefficients are defined by

$$p_{l,j} = \frac{\big|\int_{\mathcal{A}} u(\boldsymbol{x}, L)\overline{u_l^{\mathrm{OUT}}}(\boldsymbol{x})d\boldsymbol{x}\big|^2}{\int_{\mathcal{A}} |u(\boldsymbol{x}, L)|^2 d\boldsymbol{x}}. \tag{31}$$

Since $(u_l^{\mathrm{OUT}})_{l\geq 0}$ is a complete orthonormal basis of $L^2(\mathcal{A})$, the sum of these non-negative coefficients is $\sum_{l=0}^{\infty} p_{l,j} = 1$. The mode $u(\boldsymbol{x}, z = 0) = u_j^{\mathrm{IN}}(\boldsymbol{x})$ is well transmitted when $p_{j,j}$ is close to one, so we can call this coefficient the channel efficiency.

In section 4.3 we calculate the coefficients (31) using the phase screen method described in section 3.1. We also compare them with the theoretical predictions of the Itô-Schrödinger model in the weakly diffractive regime, obtained by taking the expectation in (31) and using the simple second moment formula (30),

$$\mathcal{P}_{l,j} = \iint_{\mathcal{A}^2} u_j^{\mathrm{OUT}}(\boldsymbol{x})\overline{u_j^{\mathrm{OUT}}}(\boldsymbol{x}')$$
$$\times \overline{u_l^{\mathrm{OUT}}}(\boldsymbol{x})u_l^{\mathrm{OUT}}(\boldsymbol{x}')\mathcal{K}(\boldsymbol{x}-\boldsymbol{x}')d\boldsymbol{x}d\boldsymbol{x}', \tag{32}$$

where

$$\mathcal{K}(\boldsymbol{x}) = \exp\Big[\frac{k^2\ell_z L}{4}\big(\mathcal{R}(\boldsymbol{x})-\mathcal{R}(\boldsymbol{0})\big)\Big]. \tag{33}$$

In particular, the predicted channel efficiency is

$$\mathcal{P}_{j,j} = \iint_{\mathcal{A}^2} |u_j^{\text{OUT}}(\boldsymbol{x})|^2 |u_j^{\text{OUT}}(\boldsymbol{x}')|^2 \mathcal{K}(\boldsymbol{x} - \boldsymbol{x}') d\boldsymbol{x} d\boldsymbol{x}'. \tag{34}$$

Note that since we assume identical transmitter and receiver apertures, the Rayleigh length calculated with the initial beam profile radius (15) equals the transmission distance L, so diffraction plays a role in the simulations. Nevertheless, the results in section 4.3 turn out to be in good agreement with the theoretical prediction estimates (32–34).

4.2 OAM multiplexing

Let us index the OAM modes by their topological charge $j \in \mathbb{Z}$ in the phase $\exp(ij\theta)$, which is natural for the Bessel-Gauss beams. The Laguerre-Gauss beams have a second index, but we already know from section 3 that the significant such modes (in terms of power in the aperture) are basically the same as the modes obtained with the SVD approach, discussed above. Therefore, here we focus attention on the Bessel-Gauss beams.

When the transmitter array emits the beam $u_j^{\text{BG}}(\boldsymbol{x}, z = 0)$ defined in (3), the receiver array projects the transmitted beam $u(\boldsymbol{x}, z = L)$ onto the theoretical profile $u_l^{\text{BG}}(\boldsymbol{x}, z = L)$ given by (4). This corresponds to defining the projection coefficients

$$p_{l,j}^{\text{BG}} := \frac{\left| \int_{\mathcal{A}} u(\boldsymbol{x}, L)\overline{u_l^{\text{BG}}}(\boldsymbol{x}, L)d\boldsymbol{x} \right|^2}{\int_{\mathcal{A}} |u(\boldsymbol{x}, L)|^2 d\boldsymbol{x} \int_{\mathcal{A}} |u_l^{\text{BG}}(\boldsymbol{x}, L)|^2 d\boldsymbol{x}}, \tag{35}$$

where j indexes the initial condition. Note that $\left(u_l^{\text{BG}}(\boldsymbol{x}, L)\right)_{l \in \mathbb{Z}}$ is not a complete orthonormal basis of $L^2(\mathcal{A})$, so these coefficients do not sum to one, $\sum_{l=-\infty}^{\infty} p_{l,j}^{\text{BG}} \neq 1$. We can, however, modify the definition of the coefficients to recover this normalization property [16]. The new coefficients are

$$p_{l,j}^{\text{OAM}} := \frac{\int_0^a \left| \int_0^{2\pi} u(r, \theta, L)e^{-il\theta}d\theta \right|^2 rdr}{2\pi \int_0^a \int_0^{2\pi} |u(r, \theta, L)|^2 d\theta rdr}, \tag{36}$$

and they satisfy $\sum_{l=-\infty}^{\infty} p_{l,j}^{\text{OAM}} = 1$, by Parseval's equality.

In the weakly diffractive regime we have

$$u_{j,o}^{\text{BG}}(\boldsymbol{x}) \equiv u_j^{\text{BG}}(\boldsymbol{x}, z = 0) = u_j^{\text{BG}}(\boldsymbol{x}, z = L),$$

and the theoretical predictions of the coefficients (35) and (36) given by the Itô-Schrödinger model are

$$\mathcal{P}_{l,j}^{\text{BG}} = \frac{\iint_{\mathcal{A}^2} u_{j,o}^{\text{BG}}(\boldsymbol{x})\overline{u_{j,o}^{\text{BG}}}(\boldsymbol{x}')\overline{u_{l,o}^{\text{BG}}}(\boldsymbol{x})u_{l,o}^{\text{BG}}(\boldsymbol{x}')\mathcal{K}(\boldsymbol{x} - \boldsymbol{x}')d\boldsymbol{x} d\boldsymbol{x}'}{\left[\int_{\mathcal{A}} |u_{j,o}^{\text{BG}}(\boldsymbol{x})|^2 d\boldsymbol{x} \right]\left[\int_{\mathcal{A}} |u_{l,o}^{\text{BG}}(\boldsymbol{x})|^2 d\boldsymbol{x} \right]} \tag{37}$$

14

and

$$\mathcal{P}_{l,j}^{\text{OAM}} = \frac{\mathcal{N}_{l,j}^{\text{OAM}}}{\mathcal{D}_{l,j}^{\text{OAM}}}, \tag{38}$$

$$\mathcal{N}_{l,j}^{\text{OAM}} = \int_0^a \iint_{[0,2\pi]^2} u_{j,o}^{\text{BG}}(r,\theta)\overline{u_{j,o}^{\text{BG}}}(r,\theta')$$
$$\times \mathcal{K}_{\text{OAM}}(r,\theta-\theta')e^{il(\theta'-\theta)}d\theta d\theta' r dr, \tag{39}$$

$$\mathcal{D}_{l,j}^{\text{OAM}} = 2\pi \int_0^a \int_0^{2\pi} |u_{j,o}^{\text{BG}}(r,\theta)|^2 d\theta r dr, \tag{40}$$

where $\mathcal{K}(\boldsymbol{x})$ is defined in (33) and

$$\mathcal{K}_{\text{OAM}}(r,\theta) = \exp\left[\frac{k^2\ell_z L}{4}\big(\mathcal{R}_\nu\big(2r\big|\sin(\tfrac{\theta}{2})\big|\big) - \mathcal{R}_\nu(0)\big)\right]. \tag{41}$$

For illustration, we plot in Figure 5 the coefficients $\mathcal{P}_{l,j}^{\text{OAM}}$ as a function of ℓ_c/a for $j = 1$ (left plot) and $j = 9$ (right plot). We consider various values of $\Delta = |l-j|$ and note that the sign of $l-j$ does not affect $\mathcal{P}_{l,j}^{\text{OAM}}$ in view of (3) and (39). We use $\sigma^2 k^2 \ell_z L = 8$, $r_o/a = 1$, $\beta a = 6$, $\nu = 5/6$, so that the mean field is strongly damped, but not completely vanished (see (29)), there is a strong interaction between the aperture and the initial radius, and the variations in the source Bessel function are captured within the initial radius. Similar results were obtained in [16, 22] based on a formal model for the effect of the turbulence in the form of a phase screen. Here we have put this model in the mathematical framework of beam propagation in random media, which makes explicit the scaling regime where it is valid, and we clarified the link between the phase screen parameters and those of the model for the physical medium. The figure shows that the cross talk between the modes becomes noticeable in a regime corresponding to $\ell_c \gtrsim a$. The numerical simulations in the next section are in this regime.

4.3 Numerical simulations

We now present numerical results obtained with the phase screen method described in section 3.1, for the setup in section 2.5, and the Kolmogorov-type model of the covariance obtained from definition (22). The hyperparameters in this model are $\nu = 5/6$, $\ell_c = 20$cm (i.e., $L_0 = 37$cm) and we consider three values of C_n^2 corresponding to a homogeneous medium ($C_n^2 = 0$), weak turbulence ($C_n^2 = 10^{-14}$) and stronger turbulence ($C_n^2 = 4 \cdot 10^{-14}$). These choices are similar to those in [5, 16], except for the outer scale L_0, which is smaller in our simulations. This does not have a big effect because the radius of the beams is smaller than the radius $a = 5$cm of the apertures and therefore smaller than L_0. The wavelength is $\lambda = 850$nm and the transmission distance is $L = 1$km.

The SVD based multiplexing is carried out using the SVD of the transfer matrix in the synthetic homogeneous medium. The transmitter and receiver
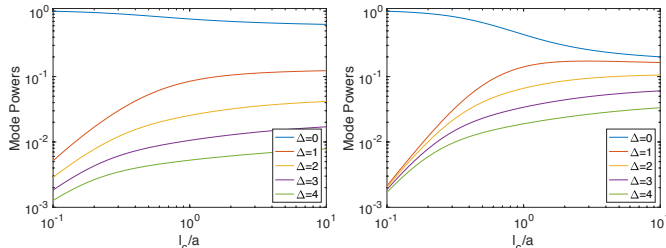
Figure 5: Theoretical prediction (38) of the projection power for $j = 1$ (left plot) and $j = 9$ (right plot) as a function of ℓ_c/a. The different curves are for the values of $\Delta = |l - j|$ shown in the legend.

aperture $\mathcal{A}$ is as in the left plot in Figure 1, so in the simulations we shift the beam axes to pass through the center $(5, 5)$cm of $\mathcal{A}$.

In the top two rows of Figure 6 we display the modulus of the beam at the receiver array, due to the initial profile given by the $j = 9$-th input SVD mode in Figure 2. The results are obtained in two realizations of the turbulent random medium, for the stronger turbulence ($C_n^2 = 4 \cdot 10^{-14}$). We also display the projection coefficients (31). As expected, the channel efficiency is perfect ($p_{j,j} = 1$) in the homogeneous medium, and it deteriorates in the turbulent medium, due to mode mixing, and the result is dependent on the realization of the medium.

Figure 7 is the analogue of Figure 6, except that the input beam is the $9-$th Bessel-Gauss mode. The main difference between Figures 6 and 7 is that the power delivered by the Bessel-Gauss beam is mostly on the edges of the aperture, whereas for the SVD mode the power is well contained inside the aperture. This plays a role for higher mode numbers, because the Bessel-Gauss modes do not take the finite aperture into account and they deliver less and less power within the receiver array. See Figure 8 for an illustration of this effect in the homogeneous medium.

The plots in Figures 6 and 7 show that the channel efficiency varies from one realization of the random medium to another. Therefore, we display in Figure 9 the mean channel efficiency obtained by averaging over 100 realizations of the random medium, and its standard deviation. The solid lines in these figures show the performance of Bessel-Gauss (black and blue lines) and SVD modes (red lines). We also plot with the dotted lines the theoretical predictions given by the Itô-Schrödinger model in the weakly diffractive regime. It appears that the low-order Bessel-Gauss modes are approximately as good as the low-order SVD modes. However, the mean channel efficiency of the Bessel-Gauss modes
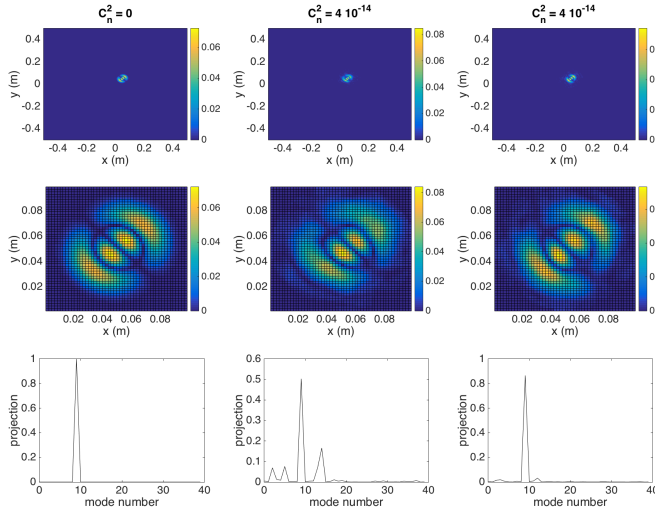
Figure 6: Here the input beam is the $j = 9$th mode obtained from the SVD. The top two rows show the transmitted field moduli at the receiver array. The second row is a zoom of the first, more exactly the values of the modulus of the field recorded by the receiver array. The axes are the coordinates in the cross-range plane, in meters. The bottom row plots the projection coefficients $p_{l,9}$ for $l = 0, \ldots, 39$. The left column is for the homogeneous transmission medium. The middle and right columns are for two realizations of the random medium with turbulence level $C_n^2 = 4 \cdot 10^{-14}$.

decreases much faster with the mode number. The channel efficiencies of the SVD modes also have smaller standard deviation.

The comparison between the red solid and dotted lines in the left plots of Figure 9 shows a good quantitative agreement between formula (32) and the numerical simulations. This is because the profiles of the transmitted SVD modes are well captured by the receiver array and the predictions of the Itô-Schrödinger model in the weakly diffractive regime are reliable. When comparing the solid and dotted black and blue lines, we observe only qualitative agreements between formulas (37-38) and the numerical simulations. This is because the profiles of the transmitted Bessel-Gauss modes are poorly captured by the receiver array (the modes are concentrated on a thin annulus which diffracts) and the predictions of the Itô-Schrödinger model in the weakly diffractive regime are then not reliable.

5 Summary

We introduced a mathematical framework for studying MIMO and OAM multiplexing for free-space optical communications between a transmitter and receiver array, using laser beams. The study takes into account the finite aper-
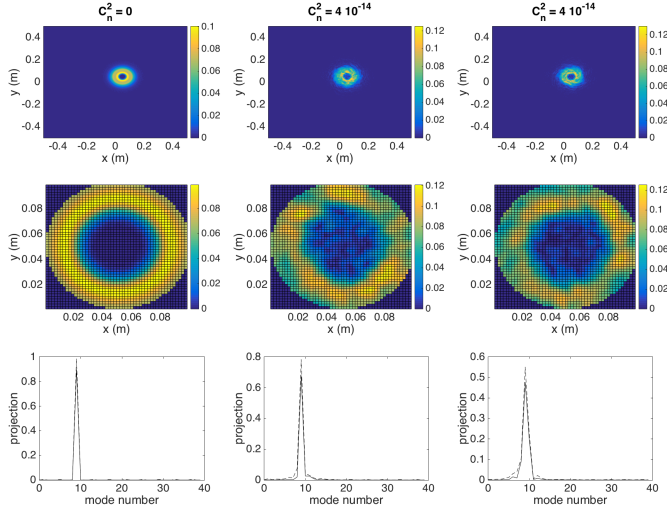
Figure 7: Here the input beam is the $j = 9$th input Bessel-Gauss mode with radius r_o given by (15). The top two rows show the transmitted field moduli at the receiver array. The second row is a zoom of the first. The axes are the coordinates in the cross-range plane, in meters. The bottom row plots the projection coefficients $p_{l,9}^{\mathrm{BG}}$ (solid line) and $p_{l,9}^{\mathrm{OAM}}$ (dashed line) for $l = 0, \ldots, 39$. The left column is for the homogeneous transmission medium. The middle and right columns are for two realizations of the random medium with turbulence level $C_n^2 = 4 \cdot 10^{-14}$.

tures of the arrays and the scattering of a turbulent transmission medium. For the commonly used circular apertures, we connected the two multiplexing approaches using the theory of prolate spheroidal functions. Explicitly, we showed that in regimes with a large number of significant singular values of the transfer matrix (i.e., many modes available for multiplexing), the MIMO approach is the same as the OAM approach for Laguerre-Gauss vortex beams, provided these have a well callibrated initial radius that depends on the wavelength, the distance of propagation and the ratio of the radii of the transmitter and receiver apertures. These communication modes are superior to other vortex beams, for example Bessel-Gauss, which do not take the finite aperture effect into account.

We used the theory of beam propagation in random media to put the phase screen numerical propagation method in a mathematical framework and to clarify the dependence of the phase screen parameters on the Kolmogorov-type model of turbulence. The theory gives theoretical estimates of the communication channel efficiency, which are compared with numerical results obtained with the phase screen method. The results demonstrate the superior performance of the SVD based multiplexing/demultiplexing approach for communication through a turbulent medium.
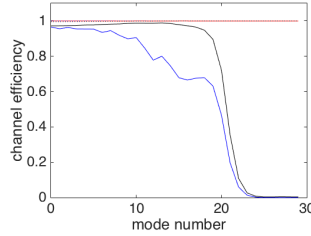
Figure 8: Channel efficiencies in the homogeneous medium: $p_{j,j}^{\mathrm{BG}}$ (solid blue) and $p_{j,j}^{\mathrm{OAM}}$ (solid black) for the Bessel-Gauss modes and $p_{j,j}$ (solid red) for the SVD modes.

Acknowledgements

References

[1] J. A. ANGUITA, M. A. NEIFELD, AND B. . VASIC, *Turbulence-induced channel crosstalk in an orbital angular momentum-multiplexed free-space optical link*, Appl. Opt., 47 (2008), pp. 2414–2429. 2

[2] S. M. BARNETT, L. ALLEN, R. P. CAMERON, C. R. GILSON, M. J. PAD-GETT, F. C. SPEIRITS, AND A. M. YAO, *On the natures of the spin and orbital parts of optical angular momentum*, J. Opt., 18 (2016), p. 064004. 2

[3] Z. BOUCHAL, *Nondiffracting optical beams: physical properties, experiments, and applications*, Czech. J. Phys., 53 (2003), pp. 537–578. 2

[4] M. CHEN, K. DHOLAKIA, AND M. MAZILU, *Is there an optimal basis to maximise optical information transfer?*, Sci. Rep., 6 (2016), p. 22821. 2

[5] T. DOSTER AND A. T. WATNIK, *Laguerre-Gauss and Bessel-Gauss beams propagation through turbulence: analysis of channel efficiency*, Appl. Opt., 55 (2016), pp. 10239–10246. 2, 3, 7, 10, 15

[6] O. EDFORS AND A. J. JOHANSSON, *Is orbital angular momentum (OAM) based radio communication an unexploited area?*, IEEE Trans. Antennas Propag., 60 (2012), pp. 1126–1131. 2

[7] J. GARNIER AND K. SØLNA, *Coupled paraxial wave equations in random media in the white-noise regime*, Ann. Appl. Probab., 19 (2009), pp. 318–346. 11, 12

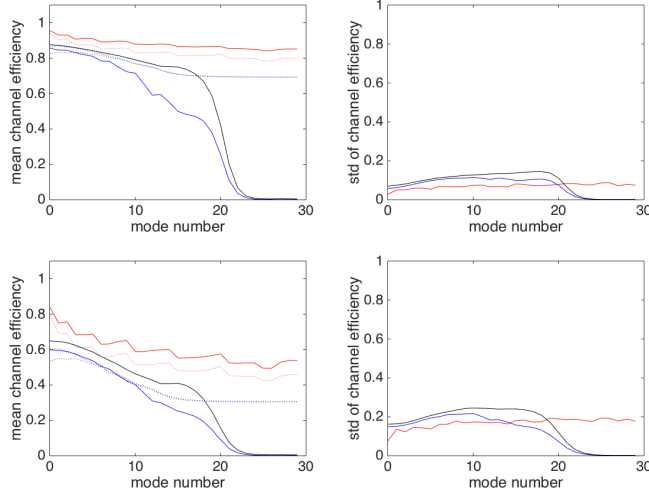Figure 9: Left: Mean channel efficiencies $p_{j,j}^{\mathrm{BG}}$ (solid blue) and $p_{j,j}^{\mathrm{OAM}}$ (solid black) for the Bessel-Gauss modes and $p_{j,j}$ for the homogeneous SVD modes (solid red). Right: Standard deviations of the channel efficiencies. Here $\sigma = 3\,10^{-9}$, $\ell_c = 20$ cm (i.e. $C_n^2 = 4\,10^{-14}$, $L_0 = 37$ cm), $a = 5$ cm, $\lambda_0 = 850$ nm, $L = 1000$ m. The dotted lines stand for the theoretical formulas (37) (dotted blue), (38) (dotted black), (32) (dotted red). Top row weak turbulence ($C_n^2 = 10^{-14}$) and bottom row stronger turbulence ($C_n^2 = 4 \cdot 10^{-14}$).

[8] G. J. GBUR, *Singular Optics*, CRC Press, Boca Raton, 2016. 2, 4, 9

[9] G. GIBSON, J. COURTIAL, AND M. J. PADGETT, *Free-space information transfer using light beams carrying orbital angular momentum*, Opt. Express, 12 (2004), pp. 5448–5456. 2

[10] F. GORI, G. GUATTARI, AND C. PADOVANI, *Bessel-Gauss beams*, Opt. Commun., 64 (1987), pp. 491–495. 2

[11] K. ITÔ, *Stochastic integral*, Proceedings of the Imperial Academy, Tokyo, 20 (1944), pp. 519–524. 12

[12] R. R. LEDERMAN, *Numerical algorithms for the computation of generalized prolate spheroidal functions*. arXiv:1710.02874. 2

[13] D. A. B. MILLER, *Waves, modes, communications, and optics: a tutorial*, Adv. Opt. Photonics, 11 (2019), pp. 679–825. 2, 3

[14] A. F. MORABITO, L. D. DONATO, AND T. ISERNIA, *Orbital angular momentum antennas: Understanding actual possibilities through the aperture antennas theory*, IEEE Antenn. Propag. M., 60 (2018), pp. 59–67. 2

[15] M. J. PADGETT AND L. ALLEN, *The Poynting vector in Laguerre-Gaussian laser modes*, Opt. Commun., 121 (1995), pp. 36–40. 5

[16] C. Paterson, *Atmospheric turbulence and orbital angular momentum of single photons for optical communication*, Phys. Rev. Lett., 94 (2005), p. 153901. 3, 10, 14, 15

[17] B. Rodenburg, *Communicating with transverse modes of light*, PhD thesis, University of Rochester, 2015. 3

[18] B. Rodenburg, M. P. J. Lavery, M. Malik, M. O'Sullivan, M. Mirhosseini, D. J. Robertson, M. Padgett, and R. W. Boyd, *Influence of atmospheric turbulence on states of light carrying orbital angular momentum*, Opt. Lett., 37 (2012), pp. 3735–3737. 2, 10

[19] J. Shapiro, S. Guha, and B. Erkmen, *Ultimate channel capacity of free-space optical communications*, J. Opt. Netw., 4 (2005), pp. 501–516. 3

[20] A. E. Siegman, *Lasers*, University Science Books, Palo Alto, 1986. 2, 3

[21] D. Slepian, *Prolate spheroidal wave functions, Fourier analysis and uncertainty - IV: Extensions to many dimensions; generalized prolate spheroidal functions*, Bell Syst. Tech. J., 43 (1964), pp. 3009–3057. 2, 3, 6, 7

[22] G. A. Tyler and R. W. Boyd, *Influence of atmospheric turbulence on the propagation of quantum states of light carrying orbital angular momentum*, Opt. Lett., 34 (2009), pp. 142–144. 3, 10, 15

[23] A. E. Willner, Y. Ren, G. Xie, Y. Yan, L. Li, Z. Zhao, J. Wang, M. Tur, A. F. Molisch, and S. Ashrafi, *Recent advances in high-capacity free-space optical and radio-frequency communications using orbital angular momentum multiplexing*, Phil. Trans. R. Soc. A, 375 (2017), p. 20150439. 2